# On the presence of high nitrite ($NO_2^-$) in coarse particles at Mt. Qomolangma

Zhongyi Zhang[1,2], Chunxiang Ye[3], Yichao Wu[1], Tao Zhou[4], Pengfei Chen[5,6], Shichang Kang[5,6], Chong Zhang[3], Zhuang Jiang[1], Lei Geng[1,2,4*]

[1]Deep Space Exploration Laboratory/School of Earth and Space Sciences, University of Science and Technology of China, Hefei 230026, Anhui, China

[2]CAS Center for Excellence in Comparative Planetology, University of Science and Technology of China, Hefei 230026, Anhui, China

[3]SKL-ESPC & SEPKL-AERM, College of Environmental Sciences and Engineering, and Center for Environment and Science, Peking University, Beijing 100871, China

[4]National Key Laboratory of Deep Space Exploration, Hefei, 230088, Anhui, China.

[5]Key Laboratory of Cryospheric Science and Frozen Soil Engineering, Northwest Institute of Eco-Environment and Resources, Chinese Academy of Sciences; Lanzhou, 730000, Gansu, China

[6]University of Chinese Academy of Sciences; Beijing, 100049, China

* *Correspondence to*: Lei Geng (Email: genglei@ustc.edu.cn; Tel: +86-0551-63600015)

## Abstract

Atmospheric reactive nitrogen cycling, with nitrous acid (HONO) and particulate nitrite ($NO_2^-$) as important intermediates, is crucial for maintaining the atmospheric oxidation capacity of background atmosphere on the Tibetan Plateau. During an eleven-day field campaign at the Base Camp of Mt. Qomolangma in spring of 2022, we observed significant enrichments of $NO_2^-$ in total suspended particulate (TSP) with a mean concentration of $375 \pm 386$ ng m$^{-3}$, while $NO_2^-$ was absent in fine particles (PM$_{2.5}$). The comparison revealed that $NO_2^-$ predominately exists in coarse particles. Local surface soil at the sampling site also exhibited high levels of $NO_2^-$, with $\delta^{15}N$ value similar to $NO_2^-$ in TSP. This isotopic similarity suggests that wind-blown soil is probably the primary source of $NO_2^-$ in TSP, accounting for the background levels. While concentration changes of water-soluble inorganic ions in TSP and PM$_{2.5}$ in response to shifts in air mass back-trajectories imply that atmospheric pollutants transported from South Asia may further elevate the $NO_2^-$, the specific mechanisms of long-range transport resulting in $NO_2^-$ accumulation in TSP rather than PM$_{2.5}$ remain unknown and need to be investigated. The elevated levels of TSP $NO_2^-$ may readily participate in atmospheric reactive nitrogen cycling through gas-particle partitioning or photolysis, leading to the production of HONO, OH and NO and thereby influencing oxidation chemistry. Further efforts on the sources and atmospheric chemistry of particulate nitrite are warranted, particularly in the pristine Tibetan Plateau, where even small inputs of $NO_x$ or HONO can disproportionately affect oxidant budgets and reactive nitrogen cycling.

# 1 Introduction

The Tibetan Plateau (TP), known as the "Third Pole", represents one of the most climate-sensitive regions on Earth (Yao et al., 2012). Over recent decades, the TP has experienced significant and rapid climate warming, primarily driven by increasing aerosol loadings and greenhouse gas concentrations due to its geographic proximity to East Asia and South Asia with intensive anthropogenic emissions (Kang et al., 2019; Lau et al., 2010; Lüthi et al., 2015). Atmospheric oxidation capacity (AOC) regulates secondary aerosol formation and trace gases removal, including $CH_4$ (Wang et al., 2023; Ye et al., 2023; Ye et al., 2016; Andersen et al., 2023), therefore acting as a critical link between atmospheric pollution and regional climate warming. Previous studies have suggested that strong solar radiation, high ozone ($O_3$) and relatively high water vapor dominate the relatively strong AOC over the TP (Lin et al., 2008). Recent field campaign further highlighted the rapid reactive nitrogen cycling, with N(III) species (i.e., HONO) as the intermediate, also plays an important role in maintaining the strong AOC in TP (Wang et al., 2023). For example, *Wang et al.* reported high-than-expected HONO (~30 ± 13 pptv) in the Namco station, a representative background site in the central TP, with identified HONO sources including $NO_2$ heterogenous conversion, soil emission and particulate nitrate photolysis (Wang et al., 2023). Incorporating the observed HONO into model simulations approximately doubled the estimated OH abundance compared to simulations without HONO constraints. However, a detailed HONO budget analysis indicated these three dominant sources could not account for the observed high daytime HONO levels at the background site, implying the existence of additional, yet unidentified, HONO sources.

Particulate nitrite ($NO_2^-$) likely represents a potential source of HONO through thermodynamic partitioning processes under favorable atmospheric conditions, provided particulate nitrite is present in significant amounts (Vandenboer et al., 2014a; Chen et al., 2019; Li, 1994). Interestingly, relatively high levels of nitrite in total suspended particulate (TSP) have also been reported from remote sites of TP, i.e., in a forest site in the Southeast Tibet ($\sim 140$ ng m$^{-3}$) and at the Qomolangma monitoring station (QOMS, $\sim 60$ ng m$^{-3}$) (Bhattarai et al., 2019; Bhattarai et al., 2023). Such high levels of particulate nitrite may also contribute to the strong AOC in TP, either via directly photolysis to produce $NO_x$ (Jacobi et al., 2014) or indirectly serve as an important source of HONO through gas-particle partitioning (R1). However, the sources and formation mechanisms for the relatively

70    high level of atmospheric $NO_2^-$ observed in the TP remain unclear.

71    $$HONO_{(g)} \leftrightarrow HONO_{(aq)} \leftrightarrow NO_2^-{}_{(aq)} + H^+{}_{(aq)} \quad (R1)$$
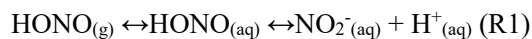
72    The stable nitrogen and oxygen isotopic compositions ($\delta^{15}N$, $\delta^{18}O$, and $\Delta^{17}O$; where $\delta =$

73    $(R_{sample}/R_{reference} - 1) \times 1000‰$ and with $R$ denoting the $^{15}N/^{14}N$, $^{18}O/^{16}O$, and $^{17}O/^{16}O$ ratios; $\Delta^{17}O =$

74    $\delta^{17}O - 0.52 \times \delta^{18}O$) may provide diagnostic information regarding the sources and formation

75    pathways of atmospheric nitrite. Similar isotopic approaches have been widely used to explore the

76    nitrate ($NO_3^-$) sources (Morin et al., 2008; Zong et al., 2020; Geng et al., 2014; Fang et al., 2011;

77    Hastings et al., 2003; Zhang et al., 2022; Zhang et al., 2021b; Liu et al., 2018; Felix and Elliott,

78    2014; Miller et al., 2018). Considering that atmospheric $NO_2^-$ may share similar sources and

79    formation pathways with $NO_3^-$, the specific $NO_2^-$ formation pathways are expected to be

80    characterized by distinct oxygen or nitrogen isotopic endmembers, despite reports on the

81    atmospheric $NO_2^-$ isotopic compositions are rare. For instance, $NO_2^-$ produced from the photolysis

82    of particulate $NO_3^-$ may possess very negative $\delta^{15}N$ values compared to $NO_3^-$, analogous to the

83    pronounced nitrogen isotope fractionation effects associated with snow nitrate photolysis (Erbland

84    et al., 2013; Frey et al., 2009), while the $\Delta^{17}O$ of $NO_2^-$ is expected to closely resemble that of $NO_3^-$

85    as the oxygen atom in $NO_2^-$ is imparted from $NO_3^-$, unless significant oxygen atom exchange

86    between $NO_2^-$ and aerosol water occurs. The $\Delta^{17}O$ of $NO_2^-$ (and HONO) from primary emission

87    sources is expected to be negligible, while that generated from heterogeneous reactions of $NO_2$ on

88    the aerosol surface would be characterized by positive $\Delta^{17}O$ values depending on the degree of $NO_2^-$

89    and aerosol water oxygen isotope exchange. These unique isotopic fingerprints may be utilized in

90    distinguishing the sources and formation pathways of atmospheric $NO_2^-$.

91    To gain insight into the sources and/or formation mechanisms of atmospheric $NO_2^-$ in the pristine

92    environment of TP, we collected the TSP and fine particulate matter ($PM_{2.5}$) synchronously at the

93    Base Camp, the north slope of the Mt. Qomolangma during the campaign of "Earth Summit

94    Mission-2022" scientific expedition from April 24th to May 6th, 2022, with additional surface soil

95    samples collected in May, 2023. The $NO_2^-$ concentration and multi-isotopic signatures ($\delta^{15}N$, $\delta^{18}O$,

96    and $\Delta^{17}O$) in aerosol and surface soil were then determined in order to evaluate the potential sources

97    of atmospheric $NO_2^-$. Additionally, the potential environmental implication of atmospheric nitrite

98    was explored in the term of atmospheric oxidation capacity at this pristine environment.

## 2 Material and Method

### 2.1 Site description

The Base Camp is located in the middle of the Rongbuk valley (86.85 °E, 28.14 °N), situated ~5200 m above sea level (m a.s.l) on the north slope of the Mt. Qomolangma (Zou et al., 2008; Zhu et al., 2006). The surrounding surface consists of loosed soil, gravel, broken rocks of various sizes, with sparse vegetation due to the semi-arid status (Ming et al., 2007; Zou et al., 2008). Rongbuk valley is characterized by a depth of ~1000 m and a floor width of ~1000 m, with elevations of the surrounding mountains exceeding 6000 m on both sides (Zou et al., 2008). Attributed to the unique topography, the local air circulation is dominated by mountain and valley breezes. The predominant wind regime is the katabatic flow of southerly and southeasterly, which is typically persists from noon to midnight (Zhu et al., 2006; Zou et al., 2008; Zhou et al., 2011). The nearest accessible area for residents and visitors is at least 2 km north of the Base Camp. During the campaign, electricity and natural gases were routinely used for cooking and hot water production. There were intermittent vehicle exhaust emissions around the station during daytime for the daily necessaries supporting, i.e., water and food. To minimize the influence of local anthropogenic activities on sampling, the instruments were set in the southeast (upwind direction, Figure S1) and approximately 100 m away from the living space of the Base Camp. The anthropogenic influence on the sampling is expected to be minimal.

### 2.2 Field campaign and sample collection

From April 26th to May 6th, 2022, TSP samples were collected simultaneously with $NO_2$ using a homemade denuder-filter system (Zhou et al., 2022). A similar system has been widely used to separately collect atmospheric particulate matter and N-containing gases for isotopic analysis (Chai et al., 2019; Chai et al., 2021), suggesting the mutual interference between the particulate and gaseous phases to be minimal. A polytetrafluoroethylene (PTFE) sleeve is used to assemble the homemade denuder with the filter pack, flowmeter, and pump. The filter pack was placed in the front of the denuder. All connections between the various parts of the sampling apparatus are made using 3/8″ Teflon tubing. A detailed description of the sampling apparatus can be found in our previous report (Zhou et al., 2022). Whatman quartz filter (circles, diam. 47mm, pre-heated at 400 ℃

127  for 3 h before use) was placed into the filter pack to collect TSP sample. In the present study, the

128  collected bulk aerosol can be regarded as TSP since no size-selective inlet was employed. The flow

129  rate was controlled at 30 Lmin$^{-1}$ using a flowmeter. Previous reports have indicated that the flow

130  rate has negligible effect on the concentrations of sulphate, nitrate, and ammonium when using

131  quartz filter for sampling (Keck and Wittmaack, 2005). To minimize the potential influence of the

132  loose ground surface on the TSP collection, a mountain tent was used to separate the pump (out the

133  tent) with the denuder-filter system (in the other side of tent), and the inlet Teflon tube was stretched

134  out of the tent for ~1.5 m height straight.

135      From April 24$^{th}$ to May 6$^{th}$, 2022, PM$_{2.5}$ were sampled using a high-volume aerosol sampler

136  (TH-1000F; Wuhan Tianhong Instruments Co. Ltd., China) equipped with PM$_{2.5}$ inlet and Whatman

137  quartz-fiber filters (sheets, 203 mm × 254 mm) at a flow rate of 1.5 m$^3$ min$^{-1}$. All the quartz filters

138  were pre-heated at 400 °C for 3 h before use. In general, TSP and PM$_{2.5}$ samples were collected with

139  diurnal resolution during this campaign, with daytime samples from approximately 09:00–20:00

140  and nighttime samples from 21:00–08:00 (local time), respectively. From May 2$^{nd}$ to May 4$^{th}$, we

141  collected the daytime TSP and PM$_{2.5}$ samples in the morning (09:00-14:00) and afternoon (14:00-

142  20:00), respectively. A total of 24 TSP samples (including 2 blanks) and 29 PM$_{2.5}$ (including 3 blanks)

143  were collected during this campaign. After each sampling period, quartz filters were removed from

144  the filter pack/PM$_{2.5}$ inlet and immediately wrapped in pre-baked aluminum foil and then stored in

145  frozen until analysis to minimize potential loss of nitrite. During the campaign, snowfall events

146  occurred on the night of April 29$^{th}$ and during the daytime of April 30$^{th}$.

147      Surface soil samples (0-5 cm depth, n = 9) were collected in May, 2023 from the east slope,

148  west slope and south sides of the Rongbuk valley. A polytetrafluoroethylene (PTFE) shovel was

149  used to collect soil. The collected soil was immediately transferred to clean plastic bags, sealed and

150  kept frozen. Soil samples were transported into laboratory using a cold chain. Upon arrival at our

151  laboratory, the soil samples were passed through a 60-mesh screen (~0.25 mm) to remove larger

152  particles and thoroughly homogenized prior to chemical and isotopic analysis.

## 2.3 Ionic concentration analysis and uncertainty estimation

154      Water-soluble inorganic ions (WSIs, including Na$^+$, NH$_4^+$, K$^+$, Mg$^{2+}$, Ca$^{2+}$, Cl$^-$, NO$_2^-$, NO$_3^-$, and

155     $SO_4^{2-}$) in TSP (entire filter, ~16.6 cm$^2$) and PM$_{2.5}$ (1/32 section, ~13.0 cm$^2$) were extracted using 20

156     mL Milli-Q ultrapure water (18.2Ω cm) in an ultrasonic bath at room temperature for 30 min. Note

157     the TSP filters were cut to fit the filter holder from the standard Whatman quartz-fiber filters which

158     were also used as the PM$_{2.5}$ filters. After filtration through a 0.22 μm pore size syringe filter which

159     was pre-cleaned with ultrapure water, the filtrate was subjected to inorganic species analysis using

160     ion chromatography (Dionex Aquion) (Zhang et al., 2020). Blank filters were pretreated and

161     measured the same as real samples, and the limits of detection (LOD) was calculated as 3 times of

162     standard deviations of blanks (Fang et al., 2015a). In general, Na$^+$ in the blank filters is comparable

163     to samples, a well-known issue for the Whatman quartz filter which is high in Na$^+$ blank. Therefore,

164     in this study, we discarded the Na$^+$ data. The volatile components (i.e., NH$_4^+$, NO$_2^-$, NO$_3^-$) and K$^+$

165     in blank are low but several times higher than the detection limits; SO$_4^{2-}$, Mg$^{2+}$ and Ca$^{2+}$ in blank

166     are significantly higher than the respective LOD but lower than samples by at least five times (the

167     lower end). All reported concentrations of each ion were blank corrected as follows:

168    
$$C_i = \frac{(\rho_{sample} - \rho_{blank}) \times V_{water} \times F}{V_{air}}$$

169     with $C_i$ representing the ambient concentrations of specie $i$ in air (ng m$^{-3}$ or μg m$^{-3}$), $\rho_{sample}$ and $\rho_{blank}$

170     are the concentrations determined by the ion chromatography (ng mL$^{-1}$), $V_{water}$ is the volume of

171     ultrapure water used for extraction (20 mL), $V_{air}$ is the volume of air sampled for each PM$_{2.5}$ or TSP

172     filter, F is the ratio of particulate matter collection area for PM$_{2.5}$ or TSP filters to the filter area used

173     for extraction.

174        The overall uncertainty in ion concentration was estimated according to the law of error

175     propagation, accounting for the sampling air volume (3% for PM$_{2.5}$ samples and 1% for TSP samples

176     as provided by the manufactures), the extraction of water volume (~0.3% for pipetting from the

177     manufacture Eppendorf), the blanks, and the analytical uncertainty from ion chromatography and

178     calibration, assuming that these factors are independent. The analytical uncertainty for water-soluble

179     ions concentration determination using ionic chromatography has been extensively assessed in our

180     laboratory, with values typically <5% for all inorganic species at concentration of 500 ng mL$^{-1}$. The

181     combined uncertainty about the ionic concentrations in PM$_{2.5}$ and TSP are shown in Table S1. In

182     general, TSP samples are associated with relatively high overall uncertainty compared to PM$_{2.5}$

183 samples, perhaps due to the relatively high blank variability from the low mass loadings in TSP.

184     For soil ionic concentration analysis, 4.0 g sieved soil was extracted using 20 mL Milli-Q

185 ultrapure water, shaken for 30min at room temperature. After centrifugation, the extract was passed

186 through 0.45 mm filters before ions analysis. The concentration determination of water-soluble

187 inorganic ions in soil extract was similar to that of aerosol samples. Detailed procedure for the

188 extraction of soil inorganic ions, especially the $NO_2^-$ has been descried in previous report (Homyak

189 et al., 2015).

190 **2.4 Isotopic analysis**

191     After concentration measurements, isotopic analyses ($\delta^{15}N$, $\delta^{18}O$, and $\Delta^{17}O$) of $NO_2^-$ in TSP

192 were conducted using the azide method (Casciotti et al., 2007). The azide method can reduce nitrite

193 ion in solution into $N_2O$ in a single step, while nitrate ion remains unchanged, ensuring no

194 interference on the nitrite isotopic analysis. The azide reagent is prepared by mixing 2 M sodium

195 azide with 40% acetic acid at a 1:1 ratio by volume in our laboratory. $NO_2^-$ standards and samples

196 were pretreated under identical conditions concerning the total volume, nitrite amount, water isotope,

197 and matrix. The $\delta^{15}N$, $\delta^{18}O$, and $\delta^{17}O$ of $N_2O$ reduced from $NO_2^-$ in the TSP samples and standards

198 were determined using a Finnigan® MAT253 plus isotope ratio mass spectrometer (IRMS) equipped

199 with a GasBench II and preconcentration system. The data calibration followed the procedures

200 described in *Albertin et al.*, 2021, using three international $KNO_2$ salt standards (RSIL-N10219,

201 RSIL-N7373, and RSIL-N23 with respective $\delta^{15}N$ and $\delta^{18}O$ values of 2.8/88.5 ‰, -79.6/4.2 ‰, and

202 3.7/11.4‰). The $\Delta^{17}O$ values of the three international references have not been certified. To address

203 this, a series laboratory experiments was conducted to determine the true values of three

204 international references in our laboratory (Zhang et al., 2025). In brief, each nitrite international

205 reference was oxidized into $NO_3^-$ by $O_3$ produced from commercial ozone generator. A parallel flow

206 of $O_3$ was also used to convert a normal $KNO_2$ salt ($\Delta^{17}O = 0$) into $NO_3^-$ to quantify the $\Delta^{17}O$ transfer

207 during $O_3$ oxidation, following the approach of (Vicars and Savarino, 2014). Based on these

208 experiments, the $\Delta^{17}O$ of RSIL-N7373 and RSIL-N23 are determined to be negligible, consistent

209 with previous findings (Albertin et al., 2021), while the $\Delta^{17}O$ of RSIL-N10219 is determined to be

210 (-9.3 ± 0.2) ‰ in our laboratory. The $^{17}O$-excess in samples is then calculated as $\Delta^{17}O = \delta^{18}O - 0.52$

211 $\times \delta^{17}O$. The standard deviations for $\delta^{15}N$, $\delta^{18}O$, $\Delta^{17}O$ of reference materials (n = 10) were determined

212  to be less than 0.1‰, 0.6‰, and 0.4‰, respectively.

213  For soil $NO_2^-$ isotopic analysis, ~30.0g sieved soil was extracted using 150 mL Milli-Q ultra-

214  pure water. The soil extract was then preconcentrated into 10 mL using ion-exchange resin before

215  isotopic analysis. The preconcentration approach was widely used for nitrate isotopic analysis in

216  snow and ice samples, and the detailed procedures and the performance have been provided in

217  *Erbland et al.,* 2013 and evaluated in our laboratory (Text S1). The concentrated soil extracts (50

218  nmol $NO_2^-$) was then subjected to soil $NO_2^-$ isotopic analysis by converting into $N_2O$ via the azide

219  method. For soil $NO_3^-$ isotopic analysis, ~5.0g sieved soil was extracted with 15 mL of 2M KCl

220  solution (Fang et al., 2015b). The remaining procedures of soil $NO_3^-$ and $NO_2^-$ analysis were same

221  as those for TSP samples, as aforementioned.

**2.5 Complementary analyses of air mass backward trajectory**

223  To evaluate the possible impact of biomass burning emissions or other pollution sources from

224  South Asia, the Hybrid Single-Particle Lagrangian Integrated Trajectory (HYSPLIT) model

225  (performed using TrajStat plugin of the MeteoInfo software) and archived Global Data Assimilation

226  System (GDAS) of meteorological data were used to model the air mass back trajectories (Wang,

227  2014). In this study, 3-day air mass backward trajectories with arriving height of 1000 m above

228  ground level were simulated to identify the most likely pathway and potential source regions of the

229  air masses at the Base Camp (Bhattarai et al., 2023; Lin et al., 2021). Moreover, the Fire Information

230  and Resource Management System (FIRMS) developed by Moderate Resolution Imaging

231  Spectrometer (MODIS) (https://worldview.earthdata.nasa.gov) was employed to identify the

232  distribution of active fire spots during the sampling period.

**3  Results**

**3.1 Mass concentrations of water-soluble inorganic ions in TSP and $PM_{2.5}$**

235  Figure 1 displays the chemical compositions of water-soluble inorganic ions, their

236  corresponding time series and fractional contributions in TSP and $PM_{2.5}$. Throughout the campaign,

237  substantial variations of total WSIs in $PM_{2.5}$ and TSP were observed. For $PM_{2.5}$ samples, the mass

238  concentrations of total WSIs before April 30th were higher than that from May 1st to May 6th (4.1 ±

239  1.7 versus 1.7 ± 0.6 µg m^{-3}; $p < 0.05$). The cut-off date of April 30th was selected based on observed

shifts in concentrations of water-soluble ions and air mass origins (described in section 4.2). This decline of total WSIs after April $30^{th}$ was predominately driven by significant reductions in secondary inorganic species, i.e., $SO_4^{2-}$, $NO_3^-$ and $NH_4^+$, with the magnitude by more than 60%. In particular, $NH_4^+$ in $PM_{2.5}$ was on average $(322 \pm 243)$ ng $m^{-3}$ before April $30^{th}$ whereas $NH_4^+$ in $PM_{2.5}$ collected during daytime and nighttime of May $1^{st}$ were 1 ng $m^{-3}$ and 3 ng $m^{-3}$, respectively, and $NH_4^+$ in $PM_{2.5}$ extractions from May $2^{nd}$ to May $6^{th}$ was below the detection limit. Therefore, the fractional contribution of secondary inorganic species in $PM_{2.5}$ also decreased (Figure 1d). Similarly, $K^+$ in $PM_{2.5}$, a good tracer of biomass burning (Ma et al., 2003), also declined significantly after April $30^{th}$ $(269 \pm 432$ versus $22 \pm 12$ ng $m^{-3}$; $p < 0.05$). The elevated concentrations of WSIs before April $30^{th}$ $(4.1 \pm 1.7 \mu g\ m^{-3})$ are comparable to previous reports at QOMS station $(4.2 \pm 2.2\ \mu g\ m^{-3})$ in the spring (Lin et al., 2021). In comparison, concentrations of $Ca^{2+}$ and $Mg^{2+}$, tracers of wind-blown dust (Wang et al., 2002), decreased by less than 20% after April $30^{th}$. In general, $SO_4^{2-}$, $NO_3^-$, and $Ca^{2+}$ are the most abundant species in $PM_{2.5}$, accounting for the majority of the mass of total WSIs. In addition, no clear diurnal variation of water-soluble inorganic ions in $PM_{2.5}$ was observed in this study (Figure S2).
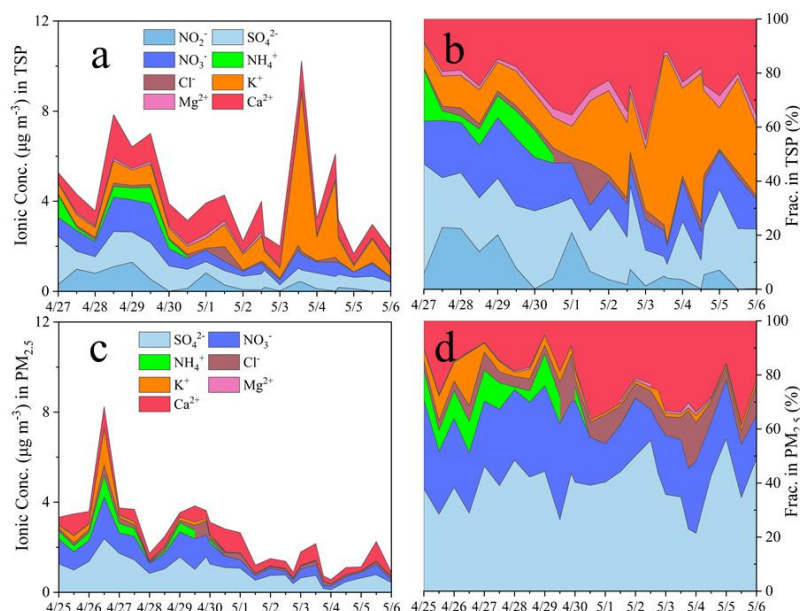
**Figure 1.** The chemical compositions and time series of mass concentrations of water-soluble inorganic species ($NO_2^-$, $SO_4^{2-}$, $NO_3^-$, $Ca^{2+}$, etc.), as well as the corresponding mass fractions in respective TSP (a, b) and $PM_{2.5}$ (c, d) samples collected at Base Camp of Mt. Qomolangma in spring 2022.

260
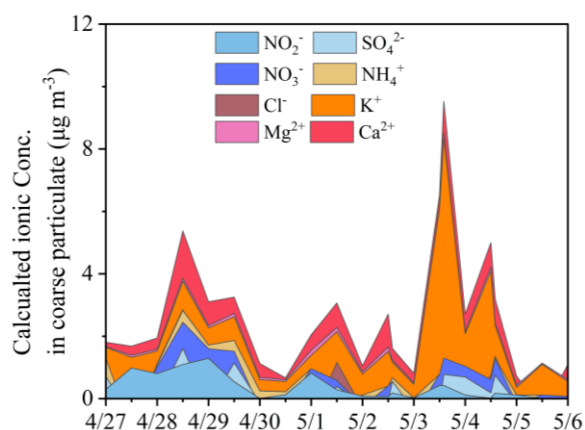
**Figure 2.** The estimated chemical compositions and time series of mass concentrations of chemical species ($NO_2^-$, $SO_4^{2-}$, $NO_3^-$, $Ca^{2+}$, etc.) in coarse-mode particulate during the springtime campaign (calculated as the difference between TSP and $PM_{2.5}$). Discontinuities in the time series were observed for certain species (e.g., $SO_4^{2-}$), likely resulting from relatively lower concentrations in the TSP samples compared to those in the corresponding $PM_{2.5}$ samples. This discrepancy is likely attributed to the propagated uncertainties involved in the concentration analysis, sampling approach and blank corrections.

Some water-soluble inorganic ions (e.g., $SO_4^{2-}$, $NO_3^-$ and $NH_4^+$) in TSP showed similar variation trends with that in $PM_{2.5}$ throughout the campaign, while others, such as $K^+$, exhibited divergent behavior (Figure 1). For example, after April 30th, the secondary inorganic species in TSP declined considerably by over 50% (i.e., $NH_4^+$ in TSP declined by more than tenfold), while $Ca^{2+}$ in TSP decreased with a smaller degree (< 15%) and $Mg^{2+}$ remained stable. In contrast, TSP $K^+$ (from both crustal and biomass burning sources)(Hsu et al., 2009) drastically surged on May 3rd and May 4th. Note that other species in TSP, i.e., $SO_4^{2-}$ and $NO_3^-$ also increased to some extent on May 3rd. The time series of water-soluble inorganic ions in the coarse-mode particulate, calculated as the differences between TSP and $PM_{2.5}$, are presented in Figure 2. Due to the overall analytical uncertainties, the air concentrations of $SO_4^{2-}$ in $PM_{2.5}$ samples occasionally exceeded that in corresponding TSP samples on some days.

Figure 3 presents the ion balance of measured water-soluble ions in $PM_{2.5}$ throughout the campaign as well as in TSP collected before and after April 30th, respectively, to highlight the significant decline in TSP $NO_2^-$. There is a strong correlation between cation and anion equivalents in $PM_{2.5}$ samples ($R^2 = 0.70$), whereas the correlations decreased in TSP samples ($R^2 = 0.46$ before April 30th and 0.49 after that, respectively). The nanogram-equivalent weights of cation were

significantly higher than that of anions for all samples, with ratio of cation to anion equivalent of ~

1.5 for $PM_{2.5}$, ~1.9 for TSP collected before April 30th, ~4.2 for TSP collected after May 1st. Clearly,

the declines in TSP $NO_2^-$ after April 30th resulted in relatively higher cation/anion equivalent ratio.

The slopes of the correlation lines exceeded unity for $PM_{2.5}$ and TSP samples, indicating the alkaline

nature of aerosol. The observed deficiency of anion can be attributed to the presence of carbonates

(i.e., $CaCO_3$), which can dissolve in water during extraction to release $CO_3^{2-}$ and/or $HCO_3^-$ despite

the relatively low solubility (Zhang et al., 2021a).

The most distinct feature of chemical compositions in TSP was the elevated level and

significant variation of $NO_2^-$, ranging from 0.2 ng m$^{-3}$ to 1291 ng m$^{-3}$ in air and with an average of

375 ± 386 ng m$^{-3}$. In comparison, $NO_2^-$ consistently remained below the detection limit in $PM_{2.5}$

samples. Note during the laboratory measurements of ionic concentrations, TSP and $PM_{2.5}$ filters

were extracted with ultrapure water and it was the extraction analyzed by ion chromatography. To

ensure fair comparisons, similar areas of filters were extracted with same volume of ultrapure water,

so that the extractions from the $PM_{2.5}$ filters should be more concentrated in atmospheric particulate

species compared to that from the TSP filters, since $PM_{2.5}$ samples were collected at a much faster

sampling speed (1.5 m$^3$ min$^{-1}$ vs. 30 L min$^{-1}$) over the same sampling duration. Nevertheless, $NO_2^-$

was detectable only in the extractions of TSP filter. The determined $NO_2^-$ concentrations in TSP in

this study (375 ± 386 ng m$^{-3}$) were higher than previous reports conducted in various remote sites,

such as at QOMS station (~60 ng m$^{-3}$ for TSP) (Bhattarai et al., 2023), at a forest site in the Southeast

Tibet Plateau (~140 ng m$^{-3}$ for TSP) (Bhattarai et al., 2019), in the middle hills of the central

Himalayas (~210 ng m$^{-3}$ for TSP) (Tripathee et al., 2021).

In particular, there was a dramatic decrease in TSP $NO_2^-$ after April 30th, from a mean of (625 ±

457) ng m$^{-3}$ to (147 ± 145) ng m$^{-3}$, in line with the declines in other secondary inorganic species.

Over the course of the campaign, $NO_2^-$ comprised approximately 8% of the total WSIs mass in TSP,

while its contribution reached maximum of ~20% on April 27th and April 28th, being one of the most

abundant components on the two days. In addition, there was a strong correlation between $NO_2^-$ and

$NO_3^-$ throughout the campaign ($r = 0.75$, $p < 0.05$. Figure S3). Meanwhile, the mean mass ratio of

$NO_2^-$ to $NO_3^-$ was ~50% throughout the campaign, but on several days (i.e., night of April 27th) $NO_2^-$

concentrations significantly exceeded that of $NO_3^-$ (802 vs. 663 ng m$^{-3}$). Previous study also reported

313    comparable $NO_2^-$ and $NO_3^-$ concentrations in at a forest site in the Southeast Tibet (summer:100 ng

314    $m^{-3}$ vs. 110 ng $m^{-3}$; winter: 180 ng $m^{-3}$ vs. 270 ng $m^{-3}$) (Bhattarai et al., 2019).

315
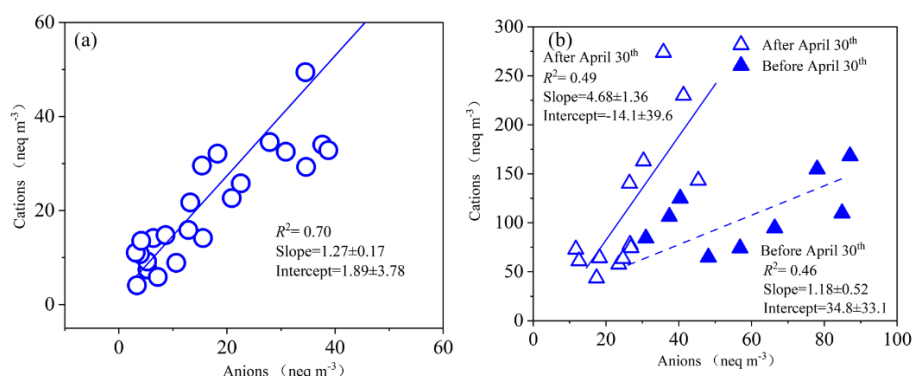
316    **Figure 3.** Ion balance for $PM_{2.5}$ (a, blue circles) and TSP samples (b, blue hollow triangles: samples

317    collected after April 30th; blue solid triangles: samples collected before April 30th). Concentrations

318    are expressed in nanogram-equivalent weight per cubic meter (neq $m^{-3}$).

319    **3.2 Isotopic signatures of nitrite in TSP**

320        Figure 4 presents the times series of $\delta^{15}N$, $\delta^{18}O$ and $\Delta^{17}O$ of $NO_2^-$ in TSP, along with the $NO_2^-$

321    concentrations. Similar to the variation trend of $NO_2^-$ concentrations, $NO_2^-$ isotopes varied in a wider

322    range before April 30th, but became more stable afterward. For example, $\delta^{15}N(NO_2^-)$ ranged from -

323    10.9 ‰ to 0.8 ‰, with a relatively large standard deviation before April 30th compared to that after

324    April 30th ((-6.4 ± 4.3) ‰ vs. (-8.0 ± 0.7) ‰). The large variability in $\delta^{15}N(NO_2^-)$ before May 1st is

325    predominately attributed to the two high values observed in daytime of April 27th and night of April

326    28th. Note that the two high $\delta^{15}N(NO_2^-)$ samples were also associated with relatively high $NO_2^-$ mass

327    concentrations. In contrast to the declining trend of $NO_2^-$ concentrations, the mean $\delta^{15}N(NO_2^-)$

328    values were comparable before and after April 30th. Relatively large variability was observed in TSP

329    $\delta^{18}O(NO_2^-)$, ranging from -9.0‰ to 3.9‰ and with an average of (-3.4 ± 3.8) ‰. TSP $\Delta^{17}O(NO_2^-)$

330    varied within a narrow range from -0.2‰ to +0.7‰ and with a mean of (0.2 ± 0.3) ‰. During the

331    campaign, no significant correlations were observed between $\delta^{15}N(NO_2^-)$ and the $NO_2^-$

332    concentrations; while $\delta^{18}O(NO_2^-)$ appeared to be moderately correlated with the $NO_2^-$

333    concentrations (Figure S5).

334
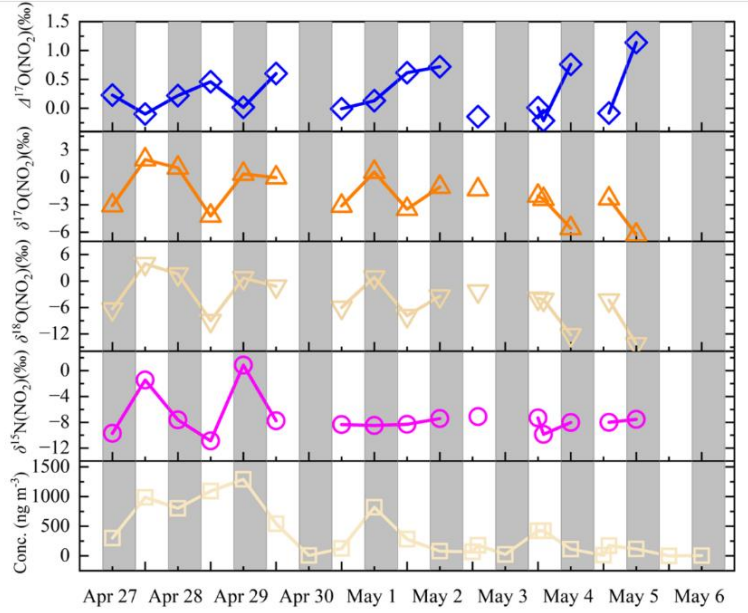
**Figure 4.** Time series of multiple isotopic signatures of $NO_2^-$ ($\delta^{15}N$, $\delta^{18}O$, $\delta^{17}O$ and $\Delta^{17}O$) as well as corresponding concentrations in TSP samples during "Earth Summit Mission" scientific expedition in spring 2022. The gray shaded area denotes local nighttime.

**Table 1.** The measured nitrite (and nitrate) concentration and isotopic signatures in surface soil collected in the Rongbuk Valley.

| Soil sample ID | $NO_2^-$ | | | | $NO_3^-$ | | | |
|---|---|---|---|---|---|---|---|---|
| | Conc.(ng g$^{-1}$) | $\delta^{15}N$ | $\delta^{18}O$ | $\Delta^{17}O$ | Conc.(ng g$^{-1}$) | $\delta^{15}N$ | $\delta^{18}O$ | $\Delta^{17}O$ |
| East-1 | 67.7 | -12.0 | 6.1 | 3.3 | 1127.3 | -2.7 | 23.4 | 5.7 |
| East-2 | 76.1 | -11.9 | 2.7 | 2.2 | 1098.3 | 1.3 | 18.1 | 3.8 |
| East-3 | 82.3 | -14.6 | 6.0 | 3.3 | 2978.1 | -0.3 | 25.4 | 6.6 |
| West-1 | 88.6 | -10.1 | 8.9 | 1.6 | 3176.5 | -3.1 | 44.5 | 13.4 |
| West-2 | 106.2 | -7.0 | 11.4 | 1.5 | 2880.3 | -1.2 | 22.1 | 6.2 |
| West-3 | 179.3 | -5.2 | 12.7 | 1.4 | 7686.9 | -3.4 | 35.8 | 11.4 |
| South-1 | 53.8 | -13.2 | 12.7 | 6.7 | 3651.2 | -0.6 | 32.6 | 10.1 |
| South-2 | 42.3 | -9.0 | 18.1 | 7.3 | 1683.2 | -2.2 | 49.3 | 14.8 |
| South-3 | 48.9 | -10.3 | 12.4 | 6.7 | 385.5 | -2.4 | 45.7 | 14.9 |

340

### 3.3 Surface soil nitrite concentration and isotopic signature

The concentration of soil $NO_2^-$ (and $NO_3^-$) as well as the corresponding isotopic signatures are displayed in Table 1. The soil $NO_2^-$ content on the west slope of Rongbuk Valley (on average 124.7 ng g$^{-1}$) was higher than that observed on the east and south sides (75.3 ng g$^{-1}$ and 48.3 ng g$^{-1}$, respectively). The mean surface soil $NO_2^-$ and $NO_3^-$ in the Rongbuk Valley were 82.8 and 2740.8 ng g$^{-1}$, respectively. The soil $NO_3^-$ concentrations were significantly higher than the $NO_2^-$ by a factor of

8 ~ 40. In general, the measured soil $NO_3^-$ concentrations at the Rongbuk valley were significantly lower than other remote regions of TP (i.e., 23.1 μg g$^{-1}$ at Naqu, 8.4μg g$^{-1}$ at Yangbajing), while soil $NO_2^-$ concentrations were comparable to these reports (i.e., 90.3 ng g$^{-1}$ at Naqu, 131.2 ng g$^{-1}$ at Yangbajing) (Wang et al., 2019). Soil $\delta^{15}N(NO_2^-)$ values ranged from -13.2‰ to -5.2‰ (on average -10.4‰), which are comparable to TSP $\delta^{15}N(NO_2^-)$ (-7.3‰). In comparison, we observed positive soil $\delta^{18}O(NO_2^-)$ and $\Delta^{17}O(NO_2^-)$, ranging from 2.7‰ to 18.1‰ (on average 10.5‰) and 1.4‰ to 7.3‰ (on average 3.8‰), respectively, in contrast to the negative $\delta^{18}O(NO_2^-)$ and near-zero $\Delta^{17}O(NO_2^-)$ observed in TSP samples. The determined soil $\delta^{18}O(NO_2^-)$ is comparable to that in laboratory incubated soil (11.8‰ ~ 12.5‰) (Lewicka-Szczebak et al., 2021).

## 4 Discussion

The significant contrast in $NO_2^-$ concentrations between TSP and $PM_{2.5}$ samples, as shown in Figure 1, suggests that at the sampling site atmospheric $NO_2^-$ overwhelmingly exists in coarse particles. This observation is consistent with previous studies across the TP, which also reported the absence of $NO_2^-$ in fine mode particles ($PM_{2.5}$ and $PM_{1.0}$) using either online real-time instrument or offline filter sampling (Decesari et al., 2010; Xu et al., 2020; Xu et al., 2023; Zhao et al., 2020), while relatively high levels of TSP $NO_2^-$ have been reported (Bhattarai et al., 2019; Bhattarai et al., 2023; Tripathee et al., 2017). In general, the chemical sources of particle $NO_2^-$ in the atmosphere encompass the uptake of HONO, particulate nitrate photolysis, and the $NO_2$-related reactions (i.e., photo-enhanced uptake of $NO_2$ on mineral dust, heterogeneous reaction of $NO_2$ on the surface of aerosol) (Nie et al., 2012; Vandenboer et al., 2014a; Chen et al., 2019; Shang et al., 2021), as summarized in Table 2. In addition to these in-situ atmospheric processes, growing evidence has revealed that long-range transport of atmospheric pollutants from South Asia also contributes considerably to aerosol loadings in TP in the spring (Kang et al., 2019; Bhattarai et al., 2023; Zhao et al., 2020), which may also bring nitrite along with other pollutants. Moreover, the lifting of surface dust can also contribute to the atmospheric coarse particles and significantly influence the chemical composition of TSP (Zhang et al., 2021a; Pokharel et al., 2019), and therefore soil nitrite could also be a potential source for TSP $NO_2^-$. In the following discussion, we examine the potential importance of the abovementioned processes to the observed high $NO_2^-$ content in coarse particle and discern the most likely ones.

**Table 2.** Particulate nitrite concentration and formation pathways/sources compiled in the literature.

| Site | Period | NO$_2^-$ Conc. (Mean, ng m$^{-3}$) | Formation pathways/Sources | Reference |
|---|---|---|---|---|
| QOMS station | April 2017 | 60 | Biomass burning emission transported from South Asia | Bhattarai et al., 2023 |
| Bakersfield, California | May–July 2010 | 150 | HONO uptake on lofted alkaline soil particles. | VandenBoer et al., 2014 |
| Jinan, China | November 2013 − January 2014 | 2080 | Heterogeneous reactions of NO$_2$ | Wang et al., 2015 |
| Seoul, Korea | May−July, 2005 | 1410 | Heterogeneous reactions of NO$_2$ | Song et al., 2009 |
| Shanghai, China | June 2020 | 210 | Heterogeneous reactions of NO$_2$, reduction of NO$_2$ by S(IV) | Shang et al., 2021 |
| Mt.Heng, China | April 2009 | 2500 | Surface TiO$_2$ photocatalysis of NO$_2$ | Nie et al., 2012 |

**4.1 The potential effects of atmospheric chemistry on NO$_2^-$ in TSP**

Increasing evidence supports particulate nitrate photolysis as an important source of atmospheric HONO especially in pristine atmosphere, with NO$_2^-$ serving as the intermediate in the subsequent gas-particle partition process (Andersen et al., 2023; Ye et al., 2016). In theory, particulate NO$_2^-$ (and HONO) produced from particulate nitrate photolysis might be associated with extremely negative $\delta^{15}$N values, due to the significant nitrogen isotopic fractionation effect during nitrate photolysis (Erbland et al., 2013; Frey et al., 2009). For example, NO$_2^-$ in water of hypersaline ponds and soil of McMurdo Dry Valleys, Antarctica, produced from the NO$_3^-$ photolysis, were characterized by significantly negative $\delta^{15}$N values (< -80‰) (Peters et al., 2014). However, $\delta^{15}$N(NO$_2^-$) in this study was only ~2‰ lower than the $\delta^{15}$N(NO$_3^-$) in TSP samples collected during this campaign (on average (-5.3 ± 3.3)‰, Text S1) and that at the QOMS stations (annual average of (-5.1 ± 2.3) ‰) (Wang et al., 2020). The similarity in $\delta^{15}$N isotopes between NO$_2^-$ and NO$_3^-$ suggests particulate nitrate photolysis is unlikely to be the primary source of the TSP NO$_2^-$.

In addition to nitrate photolysis, the absorption of HONO on alkaline aerosols (i.e., lofted dust and road salt particles) can also result in accumulation of NO$_2^-$ into the particle phase (Vandenboer et al., 2014a; Chen et al., 2019). For example, *VandenBoer et al.* observed a synchronous enhancement of fine particle NO$_2^-$ (as high as 730 ng m$^{-3}$) alongside the buildup of HONO (up to 1.37 ppbv) after sunset in an agricultural site (Vandenboer et al., 2014a). However, the levels of HONO in terrestrial background environments, typically on the order of dozens of pptv (Ye et al.,

2023), are obviously too low to support the observed unexpectedly high levels of particulate $NO_2^-$ (up to 1300 ng m$^{-3}$). What is more, previous studies indicated the HONO uptake predominately occurs on fine particles (Wang et al., 2015; Chen et al., 2019; Shang et al., 2021), while our observations indicated $NO_2^-$ only exists in coarse particles.

The uptake of $NO_2$ on mineral dust has also been identified as a significant route for the formation of particulate $NO_2^-$ or gas-phase HONO (Nie et al., 2012; Ndour et al., 2008). For example, *Nie et al.* found a significantly enhanced $NO_2^-$ in coarse particle during daytime in a dust storm event in Mt. Heng (up to 4.5 μg m$^{-3}$) (Nie et al., 2012). The proposed mechanism is initiated by photo-enhanced conversion of $NO_2$ to $NO_2^-$ via photo-produced electrons on surface of dust. Nevertheless, given the relatively small $NO_2$ uptake coefficients on mineral dust or salt surface (generally lower than $1 \times 10^{-6}$) (Yu et al., 2021; Bao et al., 2022; Xuan et al., 2025) and the low concentration of $NO_2$ in pristine environment of TP (e.g., ~ 140 pptv at Namco (Wang et al., 2023), and would be even lower at Mt. Qomolangma), such high levels of particulate $NO_2^-$ are beyond the capacity of $NO_2$ heterogeneous reactions.

Other than the above-mentioned rationales, the atmospheric physicochemical processes leading to $NO_2^-$ production would influence both fine and coarse-mode particles, and some of the processes (e.g., HONO uptake) preferentially interact with fine-mode particles. However, the observation indicated $NO_2^-$ only exists in TSP but not PM$_{2.5}$, suggesting atmospheric physicochemical processes are unlikely to account for the elevated levels of $NO_2^-$ in TSP.

**4.2 Potential effect of atmospheric pollutants in South Asia via long-range transport**

There is a growing body of compelling evidence indicating that the elevated aerosol loadings and some chemical species in TP during spring, i.e., black carbon (Cong et al., 2015; Kang et al., 2019) and soluble components (Dasari et al., 2023; Bhattarai et al., 2023; Lin et al., 2021; Wang et al., 2020; Zhao et al., 2020) are significantly linked to biomass burning emissions from South Asia, which can penetrate into TP via long range transport. Recently, *Bhattarai et al.* observed synchronously elevated water-soluble nitrogen compounds (i.e., $NO_2^-$, $NH_4^+$, $NO_3^-$), levoglucosan (a molecule marker for biomass burning) and bulk $\delta^{15}N$ signatures in TSP at QOMS station, once upon the arrival of biomass burning plumes from South Asia (Bhattarai et al., 2023). Specially, they

425  found that TSP $NO_2^-$ averaged 60 ng m$^{-3}$ during the spring biomass burning influenced episodes,

426  while $NO_2^-$ was always below the detection limit in other seasons (Bhattarai et al., 2023). This

427  suggests that biomass burning events in South Asia and the subsequent long-range transport could

428  contribute to the accumulation of $NO_2^-$ in aerosols in Tibet.

429  In this study, the mass concentrations and compositions of water-soluble ions, including $SO_4^{2-}$,

430  $NO_3^-$, $NH_4^+$ and TSP $NO_2^-$, also varied substantially throughout the springtime campaign (Figure 1).

431  The potential effect of South Asian pollutants on our observations was explored by analyzing the

432  air masses origins during the sampling period. As shown in Figure 5, during the first-half of the

433  campaign (i.e., before April 30$^{th}$), air masses predominately originated from or passed through

434  northern India and Nepal with intensive human activities and numerous fire hotspots (represented

435  by the dense red dots in Figure 5), indicating the potential impact of South Asia pollutants on aerosol

436  loadings of TP. Correspondingly, elevated concentrations of secondary inorganic ions (i.e., $NH_4^+$,

437  $NO_3^-$ and $SO_4^{2-}$) in TSP and $PM_{2.5}$ were observed before April 30$^{th}$, which are comparable to the

438  values of previous reports in QOMS station when arrived air masses experiencing severe biomass

439  burning emissions (Bhattarai et al., 2023; Lin et al., 2021). Meanwhile, elevated levels of TSP $NO_2^-$

440  (625 ± 457 ng m$^{-3}$) was observed during this biomass burning-impacted period, and $\delta^{15}N(NO_2^-)$

441  values exhibited substantial variability. TSP samples collected during daytime of April 27$^{th}$ and night

442  of April 28$^{th}$ were associated with high $NO_2^-$ concentrations and $\delta^{15}N(NO_2^-)$ values. In comparison,

443  TSP $NO_2^-$ in other samples were significantly $^{15}$N-depleted. Assuming that biomass burning

444  emission accounted for the two high $\delta^{15}N(NO_2^-)$ samples (Bhattarai et al., 2023), the observed

445  relatively low $\delta^{15}N(NO_2^-)$ in other samples before April 30$^{th}$ likely indicated the potential

446  contribution from additional emission sources.

447  From May 1$^{st}$ to May 6$^{th}$, air masses originated primarily from the inside of the TP or

448  surroundings and none of the fire hotspot was detected at the whole TP and along the air mass

449  trajectories (Figure 5), potentially excluding the influence of biomass burning and anthropogenic

450  emissions during this period. Accompanied by this significant shift in air mass origins, the

451  concentrations of $NH_4^+$, $NO_3^-$ and $SO_4^{2-}$ in both $PM_{2.5}$ and TSP, as well as the TSP $NO_2^-$ apparently

452  decreased. In particular, $NH_4^+$ in most $PM_{2.5}$ and TSP samples were below the detection limit during

453  this period. Furthermore, $K^+$ in $PM_{2.5}$, a common tracer for biomass burning, declined from 269 ±

432 ng m$^{-3}$ before April 30$^{th}$ to $22 \pm 12$ ng m$^{-3}$ after April 30$^{th}$, with the difference being statistically significant ($p < 0.05$). Meanwhile, the average TSP NO$_2^-$ also declined significantly from $625 \pm 457$ ng m$^{-3}$ before April 30$^{th}$ to $147 \pm 145$ ng m$^{-3}$ after April 30$^{th}$. Note substantially high levels of TSP NO$_2^-$ were also observed on several days after April 30$^{th}$, i.e., during daytime of May 3$^{rd}$ ($\sim 400$ ng m$^{-3}$). Although the TSP NO$_2^-$ concentrations varied in wide range after April 30$^{th}$, the $\delta^{15}N(NO_2^-)$ was relatively stable and comparable to that determined before April 30$^{th}$ (except for the two high $\delta^{15}N(NO_2^-)$ samples).

In short summary, these results likely suggest the significant impact of South Asia pollutants (i.e., biomass burning emissions) through long-range transport on the TSP NO$_2^-$, especially for samples collected before April 30$^{th}$. However, it is difficult for the long-range transport to explain why NO$_2^-$ is predominately present in coarse particles, as fine mode particle is typically easier to be transported in principle. While further studies need to be conducted to find out the exact reasons, one possibility is that the size partition of fine particle NO$_2^-$ toward the coarse mode range during transport. Similar size shifts of NO$_3^-$ have been observed and used to explain the enrichment of NO$_3^-$ in coarse-mode aerosols in marine environment (Matsumoto et al., 2009). In addition, the coarse mode particles in this study contain more alkaline species (Figure 2), which makes nitrite more stable in TSP during the transport or more stably exist in TSP after being uptake when the polluted air masses reaching TP. For the period after April 30$^{th}$, since air masses originated from clean regions with little to no biomass burning sources, other sources of nitrite might be required.

473
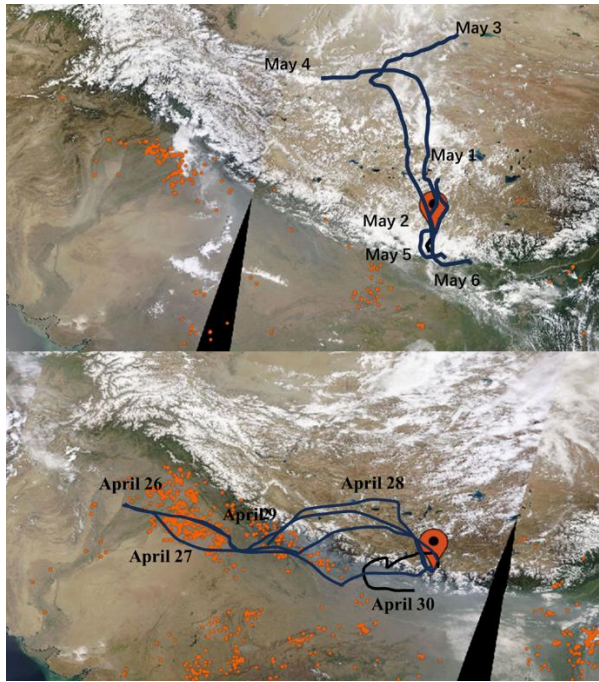
**Figure 5.** The modelled air-mass back trajectories during "Earth Summit Mission" scientific expedition in spring 2022 (a: from May 1st to May 6th; b: April 26th to April 30th). The active fire spots captured by MODIS (https://worldview.earthdata.nasa.gov, the red dots in the figure) are also presented.

**4.3 The potential effects of lofted dust**

Previous reports have confirmed that wind-blown mineral dust contributed significantly to coarse mode aerosols in TP (Kang et al., 2016; Zhang et al., 2021a). Notably, surface soil collected from the Rongbuk valley is characterized with elevated $NO_2^-$ concentration (up to 180 ng g$^{-1}$, Table 1). The surface soil $NO_2^-$ is expected to mainly reside in the coarse mode after suspended in the atmosphere (Drakaki et al., 2022), consistent with our observations that particle $NO_2^-$ was predominately confined into coarse particle. The unique environment of Rongbuk valley, characterized by exposed surface soil and strong wind (reaching as high as 9 m/s during this campaign) could facilitate the resuspension of soil components into the atmosphere. Furthermore, small localized tornadoes were frequently observed before April 30th, while the snow events occurred in April 30th would reduce the soil-derived dust emission by increasing the snow coverage and enriching the soil moisture. In fact, concentrations of $Ca^{2+}$ in TSP, which predominately originate from dust emission, also declined to some extent after April 30th.

491    In addition, the comparable $\delta^{15}N$ values of $NO_2^-$ between TSP collected after May 1st (-8.0 ±

492  0.7 ‰) and the surface soil (-10.3 ± 3.0‰) also supports that locally emitted surface soil is an

493  important contributor to the observed high levels of TSP $NO_2^-$. But one should note that the oxygen

494  isotopes ($\delta^{18}O$ and $\Delta^{17}O$) of TSP $NO_2^-$ were significantly lower compared to that in soil $NO_2^-$,

495  indicating that the original soil $NO_2^-$ oxygen isotope may have been modified after resuspension.

496  This discrepancy could be explained by the potential oxygen isotope exchanges between TSP $NO_2^-$

497  and aerosol liquid water (fractionation effect of $^{18}\varepsilon_{eq} \approx 16‰$ at local temperature, T = 270K, $^{18}\varepsilon_{eq} =$

498  $-0.12\,T + 48.79$ (Buchwald and Casciotti, 2013)), which tend to deplete both the initial $\delta^{18}O(NO_2^-)$

499  and $\Delta^{17}O(NO_2^-)$.

500     We noted the oxygen isotope exchange process between $NO_2^-$ and $H_2O$ also occurs in surface

501  soil. Previous study indicated that in high-altitude arid regions of TP (i.e., > 5000m), denitrification

502  process dominated the surface soil $NO_2^-$ production, accounting for ~75% (Wang et al., 2019). Soil

503  $NO_2^-$ generated from denitrification process is expect to inherit the $\Delta^{17}O$ signatures of substrate $NO_3^-$.

504  In this study, the surface soil $\Delta^{17}O(NO_3^-)$ were positive with average values of 9.6‰ (Table 1). The

505  positive soil $\Delta^{17}O(NO_3^-)$ have been observed on arid environments (Wang et al., 2016), such as

506  desert soil, where the low water moisture favors the preservation of atmospherically derived $NO_3^-$.

507  One could estimate that soil $\Delta^{17}O(NO_2^-)$ derived from the denitrification would be 9.6‰, nitrite

508  from other sources (e.g., nitrification) should possess zero $\Delta^{17}O$, thus in total nitrite in soil should

509  possess $\Delta^{17}O$ of ~7.2‰ (estimated as $0.75 \times \Delta^{17}O(NO_3^-)$). However, the determined soil $\Delta^{17}O(NO_2^-)$

510  (3.8‰) is significantly lower compared to the estimated soil $\Delta^{17}O(NO_2^-)$, indicating the occurrence

511  of exchange process between soil water and $NO_2^-$, which would reduce the soil $\Delta^{17}O(NO_2^-)$ to some

512  extent. The exchange process between soil water and $NO_2^-$ is particularly evident in west slope of

513  Rongbuk Valley, where soil $\Delta^{17}O(NO_2^-)$ is as low as 1.5‰ while soil $\Delta^{17}O(NO_3^-)$ is on average

514  10.3‰. Soil $\Delta^{17}O(NO_2^-)$ should be erased to near-zero if exchange process between soil water and

515  $NO_2^-$ was efficient. Therefore, the fact that the observed soil $\Delta^{17}O(NO_2^-)$ remain above 0‰ indicates

516  unfavorable conditions for the oxygen isotope exchange process, likely due to the extremely low

517  soil moisture content (~1%) in surface soil (Ma et al., 2023).

518     Upon resuspension into atmosphere, the soil-derived dust aerosols usually exhibited a certain

519  degree of hygroscopicity (Tang et al., 2016; Chen et al., 2020), allowing the absorption of water

520     molecule on dust aerosol. For example, the aerosol water was determined to account for ~20% of

521     the total $PM_{10}$ mass during Saharan dust plumes (Cardoso et al., 2018). Based on laboratory

522     experiment, Tang et al., 2019 reported that Asian dust also exhibited substantial hygroscopic

523     property and revealed that the water-soluble inorganic ions, such as $Cl^-$, $SO_4^{2-}$ and $NO_3^-$ played a

524     critical role in the absorption of water molecules on dust aerosol (Tang et al., 2019). In the present

525     study, the $SO_4^{2-}$ and $NO_3^-$ account for ~30% of the total mass of water-soluble ions in TSP, implying

526     the potential uptake of water vapor on aerosol surface. In addition to water-soluble ions, the

527     hygroscopicity of mineral dust also depends on the surface areas, and wind-blown dust experiences

528     a substantial increase in surface area after being lifted into the atmosphere, enhancing its capacity

529     for water uptake (Chen et al., 2020; Seisel et al., 2004). The hygroscopicity of dust aerosol is

530     expected to accelerate the oxygen isotope exchanges between $NO_2^-$ and aerosol liquid water. The

531     atmospheric water vapor $\delta^{18}O$ isotope in TP is determined to be significantly negative

532     (approximately -35‰ to -15‰ at a remote site in TP with altitude of ~ 4200m) (Yu et al., 2015).

533     Similarly, the oxygen isotope exchange between $NO_2^-$ and $H_2O$ would also homogenize and erase

534     original soil $\Delta^{17}O(NO_2^-)$ signals, because aerosol liquid water is characterized by negligible $\Delta^{17}O$

535     values (Luz and Barkan, 2005). Consequently, isotope exchange with aerosol water would further

536     reduce both $\delta^{18}O$ and $\Delta^{17}O$ of TSP $NO_2^-$, effectively masking the original isotopic signature inherited

537     from surface soil.

538         We also noted that $NO_2^-$ in surface soil is significantly lower than $NO_3^-$, by on average 35 times

539     (Table 1), contrasting with the chemical compositions in TSP. It is important to note that during the

540     complex dust generation and aerosolization processes, water-soluble ions exhibit significant

541     chemical enrichment relative to that in parent soil (Wu et al., 2022; Gao et al., 2023). For example,

542     Wu et al., 2022 reported that contents of nitrate in sand dust-derived $PM_{10}$ is higher than the original

543     soil samples by 2~80 times, while sulphate can be up to 500 times higher than the original soil.

544     Although the enrichment of nitrite has not been evaluated to the extent of our knowledge, we

545     propose that the observed discrepancy of nitrate/nitrite ratio between TSP and surface soil can be

546     reconciled if the nitrite is enriched more efficiently than nitrate during dust aerosolization, i.e., by a

547     factor of 30. To further assess the potential contribution of resuspended soil to elevated nitrite in

548     TSP, we conducted a rough estimation based on laboratory investigations from Wu et al. (2022).

First, the springtime TSP concentrations observed in the nearby QOMS station is used ($65.1 \pm 50.9$ $\mu g\ m^{-3}$; (Liu et al., 2017)), as TSP mass concentrations surrounding the Base camp were not available. Second, we assume the nitrite content in soil-derived coarse particles to be similar to that of nitrate (0.2%) in laboratory-generated dust aerosol from natural sandy and gravel soils (Wu et al., 2022), which is comparable to the soil texture of the Rongbuk Valley. This assumption can also explain the comparable amounts of nitrite and nitrate observed in TSP samples in this study. Results shown that the concentrations of nitrite in TSP can be approximately $130 \pm 102\ ng\ m^{-3}$, on the same order with the observed nitrite concentration in TSP after April 30th ($147 \pm 145\ ng\ m^{-3}$) but substantially lower than that before April 30th ($625 \pm 457\ ng\ m^{-3}$). Therefore, we speculate that the resuspension of surface soil may account for the observed TSP nitrite after April 30th, whereas the biomass burning and soil together co-contributed to the high TSP nitrite before April 30th. This is also consistent with the shift of air mass origins, which clearly indicated that airmasses before April 30th is significantly impacted by the biomass burning emissions, and after April 30th airmasses primarily originated from clean regions. While we acknowledge that this simplistic estimation is subject to substantial uncertainty, it provides a first-order assessment supporting the hypothesis that wind-blown soil dust contributes to coarse-mode particulate nitrite. Previously, wind-blown mineral dust has been verified as a potential source for aerosol water-soluble ions (Engelbrecht et al., 2016; Wu et al., 2022; Wu et al., 2012) and dust aerosol is also recognized as one of the important aerosol types over TP (Pokharel et al., 2019).

## 5  Conclusion and Implications

Unexpectedly high levels of $NO_2^-$ associated with coarse-particle were observed in the pristine environment at Mt. Qomolangma in the spring, 2022. After examining the potential contributions of various $NO_2^-$ sources with assistance from air mass back-trajectory and isotope analyses, we propose that both soil-derived nitrite and long-range transport of pollutants from South Asia may contribute to coarse-particle $NO_2^-$ during spring at Mt. Qomolangma. This is also consistent with previous reports showing that dust and biomass burning emissions through long-range transport from South Asia are the predominant contributors to the springtime aerosol loadings over TP (Zhao et al., 2020; Pokharel et al., 2019). The nitrite concentrations and isotopes further indicated that soil-derived nitrite likely serves as a baseline source of atmospheric $NO_2^-$, maintaining the background

levels of TSP $NO_2^-$ at this pristine site, reflected by the relatively stable isotopes when soil-derived nitrite predominated. In addition, air masses originating from South Asia would result in elevated levels of $NO_2^-$ observed before April 30th by bringing additional biomass burning and anthropogenic pollutants, as evidenced by the more varied isotopes before April 30th compared to after that day when air mass origins shifted from South Asia to central and north Tibet. However, the detailed mechanisms of nitrite enriched on the coarse particle remain unknown and need further explorations.

In the atmosphere, photolysis of particle nitrite can produce OH radical and NO, the latter is essential for the formation of atmospheric oxidants and secondary aerosols. Moreover, the elevated levels of particle $NO_2^-$ may serve as an important HONO source through the gas-to-particle partition process (Vandenboer et al., 2014a), and the thermodynamic equilibrium between particulate nitrite and HONO ([pN(III)]/[HONO] ratio) is primarily governed by the particle acidity and liquid water content (LWC) in theory (Fountoukis and Nenes, 2007; Vandenboer et al., 2014a; Chen et al., 2019). Based on the observed TSP $NO_2^-$ and estimated ratio of [pN(III)]/[HONO] (from 4.8 to 10.6, Text S2), we can estimate the potential level of atmospheric HONO if the partition ever occurs at this site (Vandenboer et al., 2014b), and result indicates HOHO would be at 8 ~ 15 pptv, on the same order with the observations at a central Tibetan site (~ 30 pptv at Namco (Wang et al., 2023)). Given that TSP concentrations usually reach maximum during spring over TP, i.e., $65 \pm 51$ μg m$^{-3}$ at the nearby QOMS station (Liu et al., 2017), our findings suggest that the coarse-particle may serve as a potential source of atmospheric HONO and $NO_x$ assuming the TSP are associated with nitrite. Although the coarse-particle tend to deposit rapidly within hours, their potential to influence local atmospheric chemistry remains important to some extent, particularly considering the frequent dust events in TP (loose arid/semiarid surface, sparse vegetation, and strong winds.(Long et al., 2025)) and the ubiquity of long-range transport of biomass burning emissions from South Asia during this season. The impact of the TSP nitrite on the budget of $NO_x$, HONO and OH radicals especially in the background atmosphere could be investigated using regional or global atmospheric transport model, once the detailed mechanism regarding the sources and chemistry of TSP nitrite been elucidated. In summary, our results highlight the need for further investigation into the sources, partitioning, and chemical reactivity of aerosol-phase nitrite, particularly in the pristine Tibetan Plateau, where even small inputs of $NO_x$ or HONO can disproportionately affect oxidant budgets

607    and reactive nitrogen cycling

608

609    **Acknowledgments** We thank Dr. Yunhong Zhou for the help in air mass back trajectory analysis.

610    The authors thank all researchers involved in the "Earth Summit Mission-2022" scientific

611    expedition from Peking University, Hefei Institutes of Physical Science Anhui Institute of Optics

612    and Fine Mechanics of Chinese Academy of Sciences, Minzu University of China.

613    **Financial support** L.G. acknowledges financial support from the National Natural Science

614    Foundation of China (Awards: 41822605 and 41871051), and the National Key R&D Program of

615    China (2022YFC3700701), the Innovation Program for Quantum Science and Technology

616    (2021ZD0303101). Z. Z acknowledges financial support from the National Natural Science

617    Foundation of China (Awards: 42273001), Key Research and Development Plan Project of Anhui

618    Province (2022l07020032). P. C acknowledges financial support from the National Natural Science

619    Foundation of China (Awards: 42371151).

620    **Conflicts of interest**

621    The authors declare that they have no conflicts of interest.

622    **Autor contribution:**

623    L.G designed the research, interpreted the data; L.G and Z.Z prepared the manuscript with

624    contributions from all co-authors; Z.Z., Y.W., C.Y., T.Z., C.Z., Z.J., and P.C., conducted the field

625    sampling and laboratory measurements; L.G, Z.Z., and P.C., acquired funding; L.G., S.K., and C.Y.

626    reviewed and edited the manuscript. All authors have given approval to the final version of the

627    manuscript.

628    **Data availability**

629    The data supporting the findings of this study are available in the archival repository at:
630    https://doi.org/10.6084/m9.figshare.28188320.v1

631    **References**

632    Albertin, S., Savarino, J., Bekki, S., Barbero, A., and Caillon, N.: Measurement report: Nitrogen isotopes
633    ($\delta^{15}$N) and first quantification of oxygen isotope anomalies ($\Delta^{17}$O, $\delta^{18}$O) in atmospheric nitrogen dioxide,
634    Atmos. Chem. Phys., 21, 10477-10497, 10.5194/acp-21-10477-2021, 2021.
635    Andersen, S. T., Carpenter, L. J., Reed, C., Lee, J. D., Chance, R., Sherwen, T., Vaughan, A. R., Stewart,

J., Edwards, P. M., and Bloss, W. J. J. S. A.: Extensive field evidence for the release of HONO from the photolysis of nitrate aerosols, Science Advances, 9, eadd6266, 2023.

Bao, F., Cheng, Y., Kuhn, U., Li, G., Wang, W., Kratz, A. M., Weber, J., Weber, B., Pöschl, U., and Su, H.: Key Role of Equilibrium HONO Concentration over Soil in Quantifying Soil–Atmosphere HONO Fluxes, Environmental Science & Technology, 56, 2204-2212, 10.1021/acs.est.1c06716, 2022.

Bhattarai, H., Wu, G., Zheng, X., Zhu, H., Gao, S., Zhang, Y.-L., Widory, D., Ram, K., Chen, X., and Wan, X.: Wildfire-Derived Nitrogen Aerosols Threaten the Fragile Ecosystem in Himalayas and Tibetan Plateau, Environmental Science Technology, 2023.

Bhattarai, H., Zhang, Y.-L., Pavuluri, C. M., Wan, X., Wu, G., Li, P., Cao, F., Zhang, W., Wang, Y., and Kang, S.: Nitrogen speciation and isotopic composition of aerosols collected at Himalayan forest (3326 m asl): seasonality, sources, and implications, Environmental Science Technology, 53, 12247-12256, 2019.

Buchwald, C. and Casciotti, K. L.: Isotopic ratios of nitrite as tracers of the sources and age of oceanic nitrite, Nature Geoscience, 6, 308-313, 10.1038/ngeo1745, 2013.

Casciotti, K. L., Böhlke, J. K., McIlvin, M. R., Mroczkowski, S. J., and Hannon, J. E.: Oxygen isotopes in nitrite: Analysis, calibration, and equilibration, Analytical Chemistry, 79, 2427-2436, 2007.

Chen, Q., Edebeli, J., McNamara, S. M., Kulju, K. D., May, N. W., Bertman, S. B., Thanekar, S., Fuentes, J. D., and Pratt, K. A.: HONO, Particulate Nitrite, and Snow Nitrite at a Midlatitude Urban Site during Wintertime, ACS Earth and Space Chemistry, 3, 811-822, 10.1021/acsearthspacechem.9b00023, 2019.

Cong, Z., Kang, S., Kawamura, K., Liu, B., Wan, X., Wang, Z., Gao, S., and Fu, P.: Carbonaceous aerosols on the south edge of the Tibetan Plateau: concentrations, seasonality and sources, Atmos. Chem. Phys., 15, 1573-1584, 10.5194/acp-15-1573-2015, 2015.

Dasari, S., Paris, G., Pei, Q., Cong, Z., and Widory, D.: Tracing the origin of elevated springtime atmospheric sulfate on the southern Himalayan-Tibetan plateau, Environmental Science: Advances, 2, 1110-1118, 2023.

Decesari, S., Facchini, M., Carbone, C., Giulianelli, L., Rinaldi, M., Finessi, E., Fuzzi, S., Marinoni, A., Cristofanelli, P., and Duchi, R. J. A. C.: Chemical composition of PM10 and PM1 at the high-altitude Himalayan station Nepal Climate Observatory-Pyramid (NCO-P)(5079 m asl), Atmospheric Chemistry Physics, 10, 4583-4596, 2010.

Drakaki, E., Amiridis, V., Tsekeri, A., Gkikas, A., Proestakis, E., Mallios, S., Solomos, S., Spyrou, C., Marinou, E., Ryder, C. L., Bouris, D., and Katsafados, P.: Modeling coarse and giant desert dust particles, Atmos. Chem. Phys., 22, 12727-12748, 10.5194/acp-22-12727-2022, 2022.

Erbland, J., Vicars, W. C., Savarino, J., Morin, S., Frey, M. M., Frosini, D., Vince, E., and Martins, J. M. F.: Air–snow transfer of nitrate on the East Antarctic Plateau Part 1: Isotopic evidence for a photolytically driven dynamic equilibrium in summer, Atmospheric Chemistry and Physics, 13, 6403-6419, 10.5194/acp-13-6403-2013, 2013.

Fang, Y., Koba, K., Wang, X., Wen, D., Li, J., Takebayashi, Y., Liu, X., and Yoh, M.: Anthropogenic imprints on nitrogen and oxygen isotopic composition of precipitation nitrate in a nitrogen-polluted city in southern China, Atmos. Chem. Phys., 11, 1313-1325, 2011.

Felix, J. D. and Elliott, E. M.: Isotopic composition of passively collected nitrogen dioxide emissions: Vehicle, soil and livestock source signatures, Atmospheric Environment, 92, 359-366, 10.1016/j.atmosenv.2014.04.005, 2014.

Fountoukis, C. and Nenes, A.: ISORROPIA II: a computationally efficient thermodynamic equilibrium model for $K^+$–$Ca^{2+}$–$Mg^{2+}$–$NH_4^+$–$Na^+$–$SO_4^{2-}$–$NO_3^-$–$Cl^-$–$H_2O$ aerosols, Atmospheric Chemistry and

Physics, 7, 4639-4659, 2007.

Geng, L., Alexander, B., Cole-Dai, J., Steig, E. J., Savarino, J., Sofen, E. D., and Schauer, A. J.: Nitrogen isotopes in ice core nitrate linked to anthropogenic atmospheric acidity change, Proceedings of the National Academy of Sciences, 111, 5808-5812, 2014.

Hastings, M. G., Sigman, D. M., and Lipschultz, F.: Isotopic evidence for source changes of nitrate in rain at Bermuda, Journal of Geophysical Research: Atmospheres, 108, 10.1029/2003jd003789, 2003.

Homyak, P. M., Vasquez, K. T., Sickman, J. O., Parker, D. R., and Schimel, J. P.: Improving nitrite analysis in soils: Drawbacks of the conventional 2M KCl extraction, Soil Science Society of America Journal, 79, 1237-1242, 2015.

Hsu, S. C., Liu, S. C., Huang, Y. T., Chou, C. C., Lung, S. C., Liu, T. H., Tu, J. Y., and Tsai, F.: Long-range southeastward transport of Asian biosmoke pollution: Signature detected by aerosol potassium in northern Taiwan, Journal of Geophysical Research: Atmospheres, 114, 2009.

Jacobi, H.-W., Kleffmann, J. r., Villena, G., Wiesen, P., King, M., France, J., Anastasio, C., and Staebler, R.: Role of nitrite in the photochemical formation of radicals in the snow, Environmental science technology, 48, 165-172, 2014.

Kang, S., Chen, P., Li, C., Liu, B., and Cong, Z.: Atmospheric aerosol elements over the inland Tibetan Plateau: Concentration, seasonality, and transport, Aerosol Air Quality Research, 16, 789-800, 2016.

Kang, S., Zhang, Q., Qian, Y., Ji, Z., Li, C., Cong, Z., Zhang, Y., Guo, J., Du, W., Huang, J., You, Q., Panday, A. K., Rupakheti, M., Chen, D., Gustafsson, Ö., Thiemens, M. H., and Qin, D.: Linking atmospheric pollution to cryospheric change in the Third Pole region: current progress and future prospects, National Science Review, 6, 796-809, 10.1093/nsr/nwz031, 2019.

Keck, L. and Wittmaack, K. J. A. E.: Effect of filter type and temperature on volatilisation losses from ammonium salts in aerosol matter, Atmospheric Environment, 39, 4093-4100, 2005.

Lau, W. K., Kim, M.-K., Kim, K.-M., and Lee, W.-S.: Enhanced surface warming and accelerated snow melt in the Himalayas and Tibetan Plateau induced by absorbing aerosols, Environmental Research Letters, 5, 025204, 2010.

Lewicka-Szczebak, D., Jansen-Willems, A., Müller, C., Dyckmans, J., and Well, R.: Nitrite isotope characteristics and associated soil N transformations, Sci Rep, 11, 5008, 2021.

Li, S. M.: Equilibrium of particle nitrite with gas phase HONO: Tropospheric measurements in the high Arctic during polar sunrise, Journal of Geophysical Research: Atmospheres, 99, 25469-25478, 1994.

Lin, Zhang, Y.-L., Yu, M., Fan, M.-Y., Xie, F., Zhang, W.-Q., Wu, G., Cong, Z., and Michalski, G.: Formation mechanisms and source apportionments of airborne nitrate aerosols at a Himalayan-Tibetan Plateau site: Insights from nitrogen and oxygen isotopic compositions, Environmental Science Technology, 55, 12261-12271, 2021.

Lin, W., Zhu, T., Song, Y., Zou, H., Tang, M., Tang, X., and Hu, J.: Photolysis of surface $O_3$ and production potential of OH radicals in the atmosphere over the Tibetan Plateau, Journal of Geophysical Research, 113, 10.1029/2007jd008831, 2008.

Liu, X.-Y., Koba, K., Koyama, L. A., Hobbie, S. E., Weiss, M. S., Inagaki, Y., Shaver, G. R., Giblin, A. E., Hobara, S., and Nadelhoffer, K.: Nitrate is an important nitrogen source for Arctic tundra plants, Proceedings of the National Academy of Sciences, 115, 3398-3403, 2018.

Lüthi, Z., Škerlak, B., Kim, S.-W., Lauer, A., Mues, A., Rupakheti, M., and Kang, S.: Atmospheric brown clouds reach the Tibetan Plateau by crossing the Himalayas, Atmospheric Chemistry Physics, 15, 6007-6021, 2015.

Luz, B. and Barkan, E.: The isotopic ratios $^{17}O/^{16}O$ and $^{18}O/^{16}O$ in molecular oxygen and their

significance in biogeochemistry, Geochimica et Cosmochimica Acta, 69, 1099-1110, 2005.

Ma, Y., Weber, R., Lee, Y. N., Orsini, D., Maxwell-Meier, K., Thornton, D., Bandy, A., Clarke, A., Blake, D., and Sachse, G.: Characteristics and influence of biosmoke on the fine-particle ionic composition measured in Asian outflow during the Transport and Chemical Evolution Over the Pacific (TRACE-P) experiment, Journal of Geophysical Research: Atmospheres, 108, 2003.

Miller, D. J., Chai, J., Guo, F., Dell, C. J., Karsten, H., and Hastings, M. G. J. G. R. L.: Isotopic composition of in situ soil NOx emissions in manure-fertilized cropland, 45, 12,058-012,066, 2018.

Ming, J., Zhang, D., Kang, S., and Tian, W.: Aerosol and fresh snow chemistry in the East Rongbuk Glacier on the northern slope of Mt. Qomolangma (Everest), Journal of Geophysical Research: Atmospheres, 112, 2007.

Morin, S., Savarino, J., Frey, M. M., Yan, N., Bekki, S., Bottenheim, J. W., and Martins, J. M.: Tracing the origin and fate of NOx in the Arctic atmosphere using stable isotopes in nitrate, Science, 322, 730-732, 10.1126/science.1161910, 2008.

Ndour, M., D'Anna, B., George, C., Ka, O., Balkanski, Y., Kleffmann, J., Stemmler, K., and Ammann, M.: Photoenhanced uptake of $NO_2$ on mineral dust: Laboratory experiments and model simulations, Geophysical Research Letters, 35, 2008.

Nie, W., Wang, T., Xue, L., Ding, A., Wang, X., Gao, X., Xu, Z., Yu, Y., Yuan, C., and Zhou, Z.: Asian dust storm observed at a rural mountain site in southern China: chemical evolution and heterogeneous photochemistry, Atmos. Chem. Phys., 12, 11985-11995, 2012.

Peters, B., Casciotti, K. L., Samarkin, V. A., Madigan, M. T., Schutte, C. A., and Joye, S. B.: Stable isotope analyses of $NO_2^-$, $NO_3^-$, and $N_2O$ in the hypersaline ponds and soils of the McMurdo Dry Valleys, Antarctica, Geochimica et Cosmochimica Acta, 135, 87-101, 2014.

Pokharel, M., Guang, J., Liu, B., Kang, S., Ma, Y., Holben, B. N., Xia, X. a., Xin, J., Ram, K., Rupakheti, D., Wan, X., Wu, G., Bhattarai, H., Zhao, C., and Cong, Z.: Aerosol Properties Over Tibetan Plateau From a Decade of AERONET Measurements: Baseline, Types, and Influencing Factors, Journal of Geophysical Research: Atmospheres, 124, 13357-13374, 10.1029/2019jd031293, 2019.

Shang, X., Kang, H., Chen, Y., Abdumutallip, M., Li, L., Li, X., Fu, H., Wang, X., Wang, L., and Wang, X.: $PM_{1.0}$-nitrite heterogeneous formation demonstrated via a modified versatile aerosol concentration enrichment system coupled with ion chromatography, Environmental Science Technology, 55, 9794-9804, 2021.

Tripathee, L., Kang, S., Rupakheti, D., Cong, Z., Zhang, Q., and Huang, J.: Chemical characteristics of soluble aerosols over the central Himalayas: insights into spatiotemporal variations and sources, Environmental Science and Pollution Research, 24, 24454-24472, 2017.

Tripathee, L., Kang, S., Chen, P., Bhattarai, H., Guo, J., Shrestha, K. L., Sharma, C. M., Sharma Ghimire, P., and Huang, J.: Water-soluble organic and inorganic nitrogen in ambient aerosols over the Himalayan middle hills: Seasonality, sources, and transport pathways, Atmospheric Research, 250, 10.1016/j.atmosres.2020.105376, 2021.

VandenBoer, T., Markovic, M., Sanders, J., Ren, X., Pusede, S., Browne, E., Cohen, R., Zhang, L., Thomas, J., and Brune, W.: Evidence for a nitrous acid (HONO) reservoir at the ground surface in Bakersfield, CA, during CalNex 2010, Journal of Geophysical Research: Atmospheres, 119, 9093-9106, 2014a.

VandenBoer, T. C., Young, C. J., Talukdar, R. K., Markovic, M. Z., Brown, S. S., Roberts, J. M., and Murphy, J. G.: Nocturnal loss and daytime source of nitrous acid through reactive uptake and displacement, Nature Geoscience, 8, 55-60, 10.1038/ngeo2298, 2014b.

Wang, J., Zhang, Y., Zhang, C., Wang, Y., Zhou, J., Whalley, L. K., Slater, E. J., Dyson, J. E., Xu, W., Cheng, P., Han, B., Wang, L., Yu, X., Wang, Y., Woodward-Massey, R., Lin, W., Zhao, W., Zeng, L., Ma, Z., Heard, D. E., and Ye, C.: Validating HONO as an Intermediate Tracer of the External Cycling of Reactive Nitrogen in the Background Atmosphere, Environ Sci Technol, 57, 5474-5484, 10.1021/acs.est.2c06731, 2023.

Wang, K., Hattori, S., Kang, S., Lin, M., and Yoshida, N.: Isotopic constraints on the formation pathways and sources of atmospheric nitrate in the Mt. Everest region, Environmental Pollution, 267, 115274, 2020.

Wang, L., Wen, L., Xu, C., Chen, J., Wang, X., Yang, L., Wang, W., Yang, X., Sui, X., and Yao, L.: HONO and its potential source particulate nitrite at an urban site in North China during the cold season, Science of the Total Environment, 538, 93-101, 2015.

Wang, S., Liu, W., Zhao, S., Wang, C., Zhuang, L., Liu, L., Wang, W., Lu, Y., Li, F., and Zhu, G.: Denitrification is the main microbial N loss pathway on the Qinghai-Tibet Plateau above an elevation of 5000 m, Science of the total environment, 696, 133852, 2019.

Wang, Y. Q. J. M. A.: MeteoInfo: GIS software for meteorological data visualization and analysis, Meteorological Applications, 21, 360-368, 2014.

Wang, Z., Akimoto, H., and Uno, I.: Neutralization of soil aerosol and its impact on the distribution of acid rain over east Asia: Observations and model results, Journal of Geophysical Research: Atmospheres, 107, ACH 6-1-ACH 6-12, 2002.

Xu, J., Hettiyadura, A. P. S., Liu, Y., Zhang, X., Kang, S., and Laskin, A.: Regional differences of chemical composition and optical properties of aerosols in the Tibetan Plateau, Journal of Geophysical Research: Atmospheres, 125, e2019JD031226, 2020.

Xu, J., Zhang, X., Zhao, W., Zhai, L., Zhao, M., Shi, J., Sun, J., Liu, Y., Xie, C., Tan, Y., Li, K., Ge, X., Zhang, Q., and Kang, S.: High-resolution physicochemical dataset of atmospheric aerosols over the Tibetan Plateau and its surroundings, Earth Syst. Sci. Data Discuss., 2023, 1-45, 10.5194/essd-2023-506, 2023.

Yao, T., Thompson, L. G., Mosbrugger, V., Zhang, F., Ma, Y., Luo, T., Xu, B., Yang, X., Joswiak, D. R., and Wang, W.: Third pole environment (TPE), Environmental Development, 3, 52-64, 2012.

Ye, C., Zhou, X., Zhang, Y., Wang, Y., Wang, J., Zhang, C., Woodward-Massey, R., Cantrell, C., Mauldin, R. L., Campos, T., Hornbrook, R. S., Ortega, J., Apel, E. C., Haggerty, J., Hall, S., Ullmann, K., Weinheimer, A., Stutz, J., Karl, T., Smith, J. N., Guenther, A., and Song, S.: Synthesizing evidence for the external cycling of NOx in high- to low-NOx atmospheres, Nature Communications, 14, 10.1038/s41467-023-43866-z, 2023.

Ye, C., Zhou, X., Pu, D., Stutz, J., Festa, J., Spolaor, M., Tsai, C., Cantrell, C., Mauldin, R. L., 3rd, Campos, T., Weinheimer, A., Hornbrook, R. S., Apel, E. C., Guenther, A., Kaser, L., Yuan, B., Karl, T., Haggerty, J., Hall, S., Ullmann, K., Smith, J. N., Ortega, J., and Knote, C.: Rapid cycling of reactive nitrogen in the marine boundary layer, Nature, 532, 489-491, 10.1038/nature17195, 2016.

Yu, C., Wang, Z., Ma, Q., Xue, L., George, C., and Wang, T.: Measurement of heterogeneous uptake of $NO_2$ on inorganic particles, sea water and urban grime, Journal of Environmental Sciences, 106, 124-135, 2021.

Yu, W., Tian, L., Ma, Y., Xu, B., and Qu, D.: Simultaneous monitoring of stable oxygen isotope composition in water vapour and precipitation over the central Tibetan Plateau, Atmospheric Chemistry and Physics, 15, 10251-10262, 10.5194/acp-15-10251-2015, 2015.

Zhang, L., Tang, C., Huang, J., Du, T., Guan, X., Tian, P., Shi, J., Cao, X., Huang, Z., and Guo, Q.: Unexpected high absorption of atmospheric aerosols over a western Tibetan Plateau site in summer,

Journal of Geophysical Research: Atmospheres, 126, e2020JD033286, 2021a.

Zhang, Y.-L., Zhang, W., Fan, M.-Y., Li, J., Fang, H., Cao, F., Lin, Y.-C., Wilkins, B. P., Liu, X., Bao, M., Hong, Y., and Michalski, G.: A diurnal story of $\Delta^{17}O(NO_3^-)$ in urban Nanjing and its implication for nitrate aerosol formation, npj Climate and Atmospheric Science, 5, 50, 10.1038/s41612-022-00273-3, 2022.

Zhang, Z., Jiang, Z., Guan, H., Liang, Y., Zheng, N., and Guo, W.: Isotopic evidence for the high contribution of wintertime photochemistry to particulate nitrate formation in Northern China, Journal of Geophysical Research: Atmospheres, 126, e2021JD035324, 2021b.

Zhang, Z., Zeng, Y., Zheng, N., Luo, L., Xiao, H., and Xiao, H.: Fossil fuel-related emissions were the major source of $NH_3$ pollution in urban cities of northern China in the autumn of 2017, Environmental Pollution, 113428, 2020.

Zhao, C., Yang, Y., Fan, H., Huang, J., Fu, Y., Zhang, X., Kang, S., Cong, Z., Letu, H., and Menenti, M.: Aerosol characteristics and impacts on weather and climate over the Tibetan Plateau, National Science Review, 7, 492-495, 2020.

Zhou, L., Zou, H., Ma, S., Li, P., Zhu, J., and Huo, C.: Vertical air mass exchange driven by the local circulation on the northern slope of Mount Everest, Advances in Atmospheric Sciences, 28, 217-222, 2011.

Zhou, T., Jiang, Z., Zhou, J., Zhao, W., Wu, Y., Yu, H., Li, W., Zhang, Z., Su, G., Ma, T., and Geng, L.: Fast and Efficient Atmospheric $NO_2$ Collection for Isotopic Analysis by a 3D-Printed Denuder System, Anal Chem, 94, 13215-13222, 10.1021/acs.analchem.2c02839, 2022.

Zhu, T., Lin, W., Song, Y., Cai, X., Zou, H., Kang, L., Zhou, L., and Akimoto, H.: Downward transport of ozone-rich air near Mt. Everest, Geophysical Research Letters, 33, 2006.

Zong, Z., Sun, Z., Xiao, L., Tian, C., Liu, J., Sha, Q., Li, J., Fang, Y., Zheng, J., and Zhang, G.: Insight into the Variability of the Nitrogen Isotope Composition of Vehicular NOx in China, Environ. Sci. Tech., 54, 14246-14253, 10.1021/acs.est.0c04749, 2020.

Zou, H., Zhou, L., Ma, S., Li, P., Wang, W., Li, A., Jia, J., and Gao, D.: Local wind system in the Rongbuk Valley on the northern slope of Mt. Everest, Geophysical Research Letters, 35, https://doi.org/10.1029/2008GL033466, 2008.

**Uncategorized References**

Cardoso, J., Almeida, S. M., Nunes, T., Almeida-Silva, M., Cerqueira, M., Alves, C., Rocha, F., Chaves, P., Reis, M., and Salvador, P.: Source apportionment of atmospheric aerosol in a marine dusty environment by ionic/composition mass balance (IMB), Atmospheric Chemistry and Physics, 18, 13215-13230, 2018.

Chai, J., Dibb, J. E., Anderson, B. E., Bekker, C., Blum, D. E., Heim, E., Jordan, C. E., Joyce, E. E., Kaspari, J. H., and Munro, H.: Isotopic evidence for dominant secondary production of HONO in near-ground wildfire plumes, Atmospheric Chemistry and Physics, 21, 13077-13098, 2021.

Chai, J., Miller, D. J., Scheuer, E., Dibb, J., Selimovic, V., Yokelson, R., Zarzana, K. J., Brown, S. S., Koss, A. R., and Warneke, C.: Isotopic characterization of nitrogen oxides (NO x), nitrous acid (HONO), and nitrate (pNO 3−) from laboratory biomass burning during FIREX, Atmospheric Measurement Techniques, 12, 6303-6317, 2019.

Chen, L., Peng, C., Gu, W., Fu, H., Jian, X., Zhang, H., Zhang, G., Zhu, J., Wang, X., and Tang, M.: On mineral dust aerosol hygroscopicity, Atmospheric Chemistry and Physics, 20, 13611-13626, 2020.

Engelbrecht, J. P., Moosmüller, H., Pincock, S., Jayanty, R., Lersch, T., and Casuccio, G.: Mineralogical, chemical, morphological, and optical interrelationships of mineral dust re-suspensions, Atmospheric

Chemistry and Physics, 16, 10809-10830, 2016.

Fang, T., Guo, H., Verma, V., Peltier, R., and Weber, R.: PM 2.5 water-soluble elements in the southeastern United States: automated analytical method development, spatiotemporal distributions, source apportionment, and implications for heath studies, Atmospheric Chemistry and Physics, 15, 11667-11682, 2015a.

Fang, Y., Koba, K., Makabe, A., Takahashi, C., Zhu, W., Hayashi, T., Hokari, A. A., Urakawa, R., Bai, E., and Houlton, B. Z.: Microbial denitrification dominates nitrate losses from forest ecosystems, Proceedings of the National Academy of Sciences, 112, 1470-1474, 2015b.

Frey, M. M., Savarino, J., Morin, S., Erbland, J., and Martins, J. M. F.: Photolysis imprint in the nitrate stable isotope signal in snow and atmosphere of East Antarctica and implications for reactive nitrogen cycling, Atmos. Chem. Phys., 9, 8681-8696, 10.5194/acp-9-8681-2009, 2009.

Gao, Q., Zhu, S., Zhou, K., Zhai, J., Chen, S., Wang, Q., Wang, S., Han, J., Lu, X., and Chen, H.: High enrichment of heavy metals in fine particulate matter through dust aerosol generation, Atmospheric Chemistry and Physics, 23, 13049-13060, 2023.

Liu, B., Cong, Z., Wang, Y., Xin, J., Wan, X., Pan, Y., Liu, Z., Wang, Y., Zhang, G., Wang, Z., Wang, Y., and Kang, S.: Background aerosol over the Himalayas and Tibetan Plateau: observed characteristics of aerosol mass loading, Atmospheric Chemistry and Physics, 17, 449-463, 10.5194/acp-17-449-2017, 2017.

Long, H., Cheng, L., Yang, F., and Zhang, G.: Temperature regulates dust activities over the Tibetan Plateau, The Innovation, 6, 2025.

Ma, Y., Xie, Z., Ma, W., Han, C., Sun, F., Sun, G., Liu, L., Lai, Y., Wang, B., and Liu, X.: QOMS: a comprehensive observation station for climate change research on the top of Earth, Bulletin of the American Meteorological Society, 104, E563-E584, 2023.

Matsumoto, K., Minami, H., Uyama, Y., and Uematsu, M.: Size partitioning of particulate inorganic nitrogen species between the fine and coarse mode ranges and its implication to their deposition on the surface ocean, Atmospheric Environment, 43, 4259-4265, 2009.

Seisel, S., Lian, Y., Keil, T., Trukhin, M. E., and Zellner, R.: Kinetics of the interaction of water vapour with mineral dust and soot surfaces at T= 298 K, Physical Chemistry Chemical Physics, 6, 1926-1932, 2004.

Tang, M., Cziczo, D. J., and Grassian, V. H.: Interactions of Water with Mineral Dust Aerosol: Water Adsorption, Hygroscopicity, Cloud Condensation, and Ice Nucleation, Chemical Reviews, 116, 4205-4259, 10.1021/acs.chemrev.5b00529, 2016.

Tang, M., Zhang, H., Gu, W., Gao, J., Jian, X., Shi, G., Zhu, B., Xie, L., Guo, L., and Gao, X.: Hygroscopic properties of saline mineral dust from different regions in China: Geographical variations, compositional dependence, and atmospheric implications, Journal of Geophysical Research: Atmospheres, 124, 10844-10857, 2019.

Vicars, W. C. and Savarino, J.: Quantitative constraints on the $^{17}O$-excess ($\Delta^{17}O$) signature of surface ozone: Ambient measurements from 50°N to 50°S using the nitrite-coated filter technique, Geochimica et Cosmochimica Acta, 135, 270-287, 10.1016/j.gca.2014.03.023, 2014.

Wang, F., Ge, W., Luo, H., Seo, J.-H., and Michalski, G.: Oxygen-17 anomaly in soil nitrate: A new precipitation proxy for desert landscapes, Earth and Planetary Science Letters, 438, 103-111, 2016.

Wu, F., Zhang, D., Cao, J., Xu, H., and An, Z.: Soil-derived sulfate in atmospheric dust particles at Taklimakan desert, Geophysical research letters, 39, 2012.

Wu, F., Cheng, Y., Hu, T., Song, N., Zhang, F., Shi, Z., Hang Ho, S. S., Cao, J., and Zhang, D.: Saltation–

900  sandblasting processes driving enrichment of water-soluble salts in mineral dust, Environmental Science
901  & Technology Letters, 9, 921-928, 2022.
902  Xuan, H., Liu, C., Zhang, P., Chu, B., Liang, L., Ma, Q., and He, H.: A Review of Laboratory Studies on
903  the Heterogeneous Chemistry of NO2: Mechanisms and Uptake Kinetics, The Journal of Physical
904  Chemistry A, 2025.
905  Zhang, Z., Zhou, T., Jiang, Z., Ma, T., Su, G., Ruan, X., Wu, Y., Cao, Y., Wang, X., Liu, Z., Li, W., Zhang,
906  H., Lin, M., Liu, P., and Geng, L.: High-Resolution Measurements of Multi-Isotopic Signatures ($\delta^{15}$N,
907  $\delta^{18}$O, and $\Delta^{17}$O) of Winter NO$_2$ in a Megacity in Central China, Environmental Science & Technology,
908  59, 3634-3644, 10.1021/acs.est.4c07724, 2025.
909